Strong S_1-S_2 Vibronic Coupling and Enhanced Third Order Hyperpolarizability in the First Excited Singlet State of Diphenylhexatriene Studied by Time-Resolved CARS

W. Werncke,* S. Hogiu, M. Pfeiffer, A. Lau, and A. Kummrow

Max-Born-Institut für Nichtlineare Optik und Kurzzeitspektroskopie, Max-Born-Strasse 2A, D-12489 Berlin, Germany

Received: August 11, 1999; In Final Form: February 1, 2000

A strong S_1-S_2 vibronic coupling effect is observed in the time-resolved coherent anti-Stokes Raman spectroscopy (CARS) spectra originating from the first excited singlet state of diphenylhexatriene. As determined from picosecond CARS measurements, the excited state spectrum appears on a subpicosecond time scale. An extremely high excited state hyperpolarizability $|\gamma|_{\text{excited state}} \cong 3 \times 10^{-31}$ is derived from a CARS line shape analysis and is attributed to the increased delocalization after excitation in accordance with semiempirical calculations of bond lengths. We observe two strongly frequency-broadened vibrations being upshifted with respect to the C═C double bond stretching region of the ground state and assign them to the totally symmetric C═C stretching motion of the chain. Both frequencies depend on the solvent polarizability, giving evidence of strong S_1-S_2 vibronic coupling in the lowest excited singlet states. We discuss a model of S_1-S_2 vibronic coupling via an asymmetric low frequency mode. According to this model a double-well potential for the respective vibrational coordinate is generated in the first excited singlet state, resulting in two frequencies originating from the same type of vibration.

1. Introduction

Polyenes have attracted a great deal of attention because of their role in vision[1] and in photosynthesis.[2−4] The function of these molecules is to absorb light and to participate in the subsequent intra- and intermolecular conversion processes to the final acceptors. As internal energy redistribution is mainly accompanied by vibronic coupling, investigation of these effects should be a key for an improved understanding of these processes. Potential technical applications of polyenes are expected using the high third order optical nonlinearity γ in the electronic ground state.[5−7] It has been reported that γ can be further increased after electronic excitation; however, those measurements have remained scarce.[8,9] In this paper we will demonstrate that coherent Raman spectroscopy is well suited to study both aspects, vibronic coupling as well as optical nonlinearity.

Since for about twenty years it is known that the totally symmetric C═C stretching vibration of the polyenic chain strongly couples the $1A_g$ and $2A_g$ electronic states[10−14] which represent, in not too short polyenes, the S_0 and S_1 states, respectively. Vibronic coupling causes the vibrational frequency of this vibration in the electronic ground state to be shifted down, and in the higher electronic potential to be shifted up by an amount of ca. 100 wavenumbers. The anomalously strong shift beyond the range of the C═C stretching frequencies can be described without assuming any changes of the corresponding bond orders.[11]

The optical transition between the $1A_g$ and the $2A_g$ electronic states is not allowed because of symmetry reasons. Recently it has been shown quantitatively that the radiationless $2A_g-1A_g$ transfer rate in β-carotene is directly related to the vibronic coupling strengths of the C═C stretching mode, i.e., vibronic coupling of this mode plays a dominant role in $2A_g-1A_g$ internal conversion.[15] Internal conversion between the primarily optically pumped $1B_u$ (S_2) level to the $2A_g$ (S_1) level is even faster than the $2A_g-1A_g$ transfer occurring on a femtosecond time scale.[16] The mechanisms involved in this fast transfer are not fully understood.[3] The energy gap between $1B_u$ and $2A_g$ is much smaller than that between $2A_g$ and $1A_g$ favoring vibronic coupling effects. However, in symmetric polyenes coupling of these two excited states by an a_g mode, e. g., by the totally symmetric C═C stretching mode, should not be effective because of symmetry reasons. In contrast it has been shown that in diphenylbutadiene investigated in the gas phase the optical forbidden transition between $1A_g$ and $2A_g$ gains oscillator strength from the allowed $1A_g-1B_u$ transition via $1B_u-2A_g$ vibronic coupling by a low frequency b_u mode.[17] Consequently asymmetric low frequency modes should be taken into account for $1B_u-2A_g$ vibronic coupling in other polyenes, too. $1B_u-2A_g$ vibronic coupling effects of the totally symmetric C═C stretching vibration of the chain have been observed not only in the first excited state of asymmetric polyenes but also in β-carotene.[18] The latter case was explained by symmetry distortions.

Because of their chemical stability the series of diphenyl polyenes is a suitable model for studying vibronic coupling.[19,20] As in other (not too short) polyenes the optically accessible $1B_u$ state (S_2) is located above the $2A_g$ electronic state (S_1), and the gap becomes closer with decreasing chain lengths[21] and almost disappears in the case of diphenylhexatriene (DPH). Furthermore the low gap can be tuned significantly in changing the polarizability of the solvent.[22] Thus DPH gives the unique possibility to study S_1-S_2 vibronic coupling effects under the extreme condition of a very small gap.

Recently we reported on a S_1-S_2 vibronic coupling effect in the first excited singlet state of DPH which we observed by time-resolved CARS.[23,24] It was explained by $2A_g-1B_u$ vibronic coupling by two active coupling vibrational modes of b_u and a_g

* Corresponding author phone/fax:+49−30−63921413/1429. E-mail: werncke@mbi-berlin.de

10.1021/jp992839a CCC: $19.00
Published on Web 03/30/2000

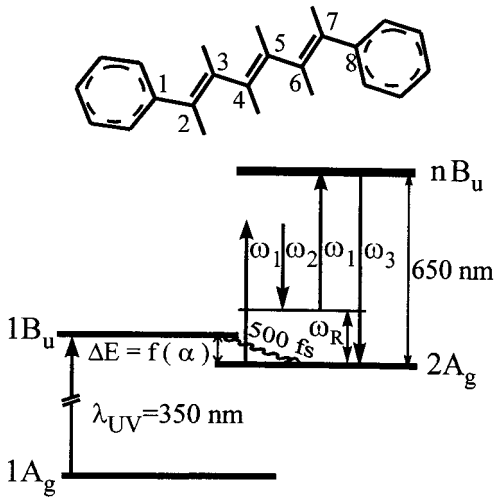

Figure 1. Molecular structure of diphenylhexatriene (DPH). Photoexcitation to the $1B_u$ state by a pulse at $\lambda_{UV} \cong 350$ nm and CARS probing of a vibrational resonance ω_R of the excited electronic state are illustrated. For simplicity the excited state absorption is indicated as a $2A_g-nB_u$ transition only.

symmetry, respectively.[25] In this paper we further extend the study of the properties of the first excited electronic state of DPH. From the CARS spectra we determine the excited state third order hyperpolarizability and discuss the results from the viewpoint of molecular geometries which we calculated semiempirically for the electronic ground and for the lowest two excited electronic states, respectively. The huge excited state third order hyperpolarizability can be rationalized by an increased delocalization within the π-chain compared to the electronic ground state. We observe two strongly upshifted vibrations appearing on a subpicosecond time scale simultaneously after electronic excitation. According to our assignment, these vibrational frequencies belong to the totally symmetric C═C stretching motion of the excited chain. Their frequency dependence on the solvent polarizability gives evidence of a strong S_1-S_2 vibronic coupling effect in the lowest excited singlet state. Frequency shifts as well as frequency broadening can be explained by coupling via asymmetric low frequency mode(s), changing the potential for their vibrational motion and resulting in two minima for the corresponding excited state potential.

2. Photophysics of Diphenylhexatriene

The molecular structure of DPH is depicted in Figure 1. The lowest band in the absorption spectrum is due to a S_0-S_2 transition to the $1B_u$ state near 350 nm. Deactivation to the lowest excited $2A_g$ state occurs on a 500 fs time scale as being determined by the changed transient absorption signal near 650 nm[26] (see Figure 1). The assignment of this transient absorption around 650 nm to excited state electronic transitions is not quite clear. Assignments to both the $2A_g-nB_u$ as well as the $1B_u-nA_g$ transitions have been given,[26,27] and it has been argued that the lowest excited singlet has some B_u character as well.[28] The gap ΔE between the two excited states is about 1000 cm^{-1} [29] and can be varied by about 500 cm^{-1} in choosing solvents of different polarizability α.[22] The lifetime of the lowest excited electronic state has been measured by time-resolved fluorescence spectroscopy showing single-exponential decay with $\tau = 13.1$ ns in a cyclohexane solution.[30]

In Figure 1, the wavelength for photoexcitation at λ_{UV} and the frequencies for CARS probing at (ω_1, ω_2, ω_3) near the transient absorption around 650 nm are shown schematically. CARS probing is carried out near the transient absorption to obtain a selective resonance enhancement for detection of the vibrations originating from the excited electronic state.

3. Experimental Section

The experimental apparatus has been described in detail elsewhere.[23] Briefly, the frequency doubled radiation of a mode-locked Nd:YAG laser is used for synchronously pumping a dye laser delivering pulses of 1.5−8 ps at 76 MHz repetition rate at 710 nm. These pulses were amplified up to 100 μJ by a three stage dye amplifier pumped by the frequency doubled pulses of a regenerative amplifier. The repetition rate of the latter was 50 Hz. Either pulses of the frequency-doubled dye laser radiation or the third harmonic of the regenerative amplifier were used for photoexcitation of the DPH sample. For CARS generation, a small portion (5%) of the dye laser pulse was mixed with the radiation of a broad band dye laser which was directly pumped by the second harmonic radiation of the regenerative amplifier. Broad band CARS signals obtained in this way were recorded after spatial filtering by a polychromator with a liquid nitrogen cooled CCD camera. Spectra were recorded without and with additional UV radiation with different delays between UV excitation and CARS probing. In addition, we recorded CARS spectra of a thin (0.5 mm) glass plate. In the frequency range 1000 to 2000 cm^{-1} this CARS spectrum is dominated by the constant electronic contribution of glass γ, and as a consequence reproduces the spectral distribution of the broad band dye laser. Displayed spectra are normalized to this reference unless otherwise stated.

Most investigations were carried out with parallel polarization between all beams. For determination of frequencies of very broad vibrational bands we additionally applied the scheme of polarization-sensitive CARS[24,31,38,39] to suppress interferences with the electronic background in the spectra. Here the polarization vectors of the laser radiation with the frequencies ω_1 and ω_2 form an angle of $\phi = 71.5°$ with each other. Depending on the Raman depolarization ratios ρ_R of the vibrational modes, the vibrational polarization vectors and the polarization vector P^E of the electronic contribution of the third order hyperpolarizability are in general all different. The polarization properties of the CARS signal are analyzed by a polarizer in front of the polychromator. Tuning the angle of the analyzer perpendicular to P^E results in the pure vibrational contributions, however, on a much lower signal level. We used circularly polarized UV excitation and rather long delay times (50 ps) to avoid an anisotropic distribution of molecules in the experiment. Measurements of the third order hyperpolarizability in the first excited state of DPH have been carried out by a nanosecond apparatus with simultaneous 355 nm excitation as described in ref 32.

Commercially available DPH was used without further purification and was dissolved in solvents of spectrograde quality. Time-resolved spectroscopic measurements were carried out in rotating sample cells to minimize photodegradation in the irradiated volume.

4. Determination of Molecular Data from the CARS Spectra

The CARS signal $I_3(-\omega_3, \omega_1, \omega_1, -\omega_2)$, being generated by simultaneous irradiation of a laser pulse $I_1(\omega_1)$ having a fixed frequency ω_1 and of a second spectrally broad pulse $I(\omega_2)$ centered around ω_2, contains more information than the corresponding spontaneous Raman spectrum. In addition to Raman

frequencies, intensities, and phases, the third-order electronic hyperpolarizabilities γ can be derived. After dividing through the spectral distribution of the CARS spectrum of the glass plate (for taking into account the spectral distribution of the broad band dye laser), the normalized CARS spectrum $I_3^N(-\omega_3, \omega_1, \omega_1, -\omega_2)$ is obtained. In a neat medium it results from the modulus squared of the overall (molecular) third-order hyperpolarizability γ[FWM 33]

$$I_3^N(-\omega_3, \omega_1, \omega_1, -\omega_2) \propto |\gamma^{FWM}(-\omega_3, \omega_1, \omega_1, -\omega_2)|^2 = \left|\gamma + \sum_R \frac{\gamma^R}{\delta_R + i\Gamma_R}\right|^2 \quad (1)$$

CARS is measured at the signal frequency $\omega_3 = 2\omega_1 - \omega_2$ around $\delta_R = \omega_R - \omega_1 + \omega_2$. $|\gamma^R|/\Gamma_R$ is the Raman amplitude of the mode with the vibrational frequency ω_R and line width Γ_R. The susceptibilities γ and γ^R are constants, or, in the case of electronic resonance, they vary very slowly within the range of a Raman spectrum (depending on the detuning of the excitation frequencies from the comparatively broad electronic transitions.[34] In nonabsorbing materials, such as most solvents used, laser frequencies are far from electronic resonance. In this case γ and γ^R are real valued quantities. Near electronic resonance they become complex valued.[35,36]

The total coherent Raman four-wave mixing spectrum at $\omega_3 = 2\omega_1 - \omega_2$ for a solute (which may be also a short-living transient) in a solution reads

$$I_3^N(-\omega_3, \omega_1, \omega_1, -\omega_2) \propto |(1-c)\gamma_{solvent}^{FWM} + c\gamma_{solute}^{FWM}|^2 \quad (2)$$

Here $c = N_{solute}/(N_{solute} + N_{solvent})$ is the relative concentration of the solute, (N: number of molecules per cm^3). It is obvious from eqs 1 and 2 that the CARS spectrum contains interference terms between the different contributions. As a consequence, an isolated vibrational resonance is characterized by a constant (electronic) background (amplitude A), by a positive or negative dispersion-like shaped contribution (B), and by a Lorentzian shaped contribution (C)

$$I_3(\delta_R) \propto A + \frac{\delta_R B + C}{\delta_R^2 + \Gamma_R^2} \quad (3)$$

A non vanishing parameter C results either in a peak or in a dip, depending on its sign. Dips (i.e., $C < 0$) are generated with complex parameters only, indicating electronic resonance.

Due to interference with the electronic background, a vibrational frequency coincides neither exactly with the peaks nor with the dips in the spectra (see eq 3). A fitting procedure as outlined in section 5 is applied to get Raman frequencies, intensities, and phases as well as the electronic contribution to the hyperpolarizability. For a detailed discussions of CARS line shape analysis see refs 35 and 36.

5. Results

An excited state CARS spectrum of DPH dissolved in cyclohexane (2×10^{-3} mol/L) recorded with 20 ps delay after UV excitation in the frequency range 1050 to 1950 cm^{-1} is shown in Figure 2 (line I) together with the corresponding spontaneous resonance Raman spectrum of the electronic ground state (2×10^{-4} mol/L, line II). The latter was recorded with 334.5 nm excitation. The inset of Figure 2 shows the low frequency resonance Raman spectrum together with the corresponding spectrum of the pure solvent corrected by the Bose−Einstein factor $[\exp(h\omega/2\pi k_B T) - 1]^{-1} + 1$, where ω is the vibrational frequency and k_B is the Boltzmann constant. The most prominent feature in the low frequency Raman spectrum (solid line) is a line near 35 cm^{-1} of DPH (indicated by arrow). It can be clearly distinguished from the low frequency Raman contribution of pure cyclohexane at 29 cm^{-1} (marked by asterisks in the dashed line).

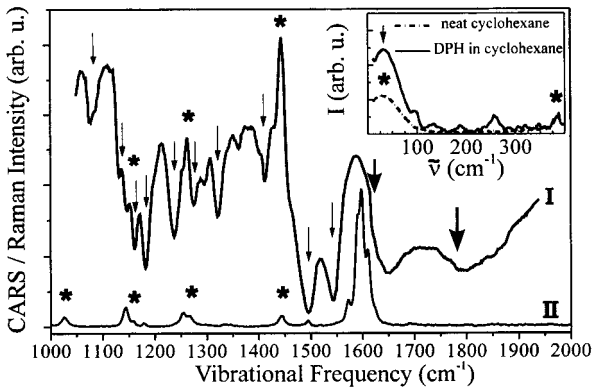

Figure 2. Comparison of the CARS spectrum of DPH in the first excited singlet state (line I) recorded 20 ps after UV excitation (2×10^{-3} mol/L DPH solution in cyclohexane, $\lambda_{UV} = 355$ nm, $\lambda_1 = 710$ nm) with the corresponding resonance Raman spectrum of the electronic ground state (line II) recorded at 334.5 nm. Vibrational resonances of DPH after excitation are indicated by arrows, the thick arrows indicate the two unusual upshifted Raman bands, solvent lines are marked by asterisks. A low frequency resonance Raman spectrum of DPH (dissolved 2×10^{-4} mol/L in cyclohexane) in the electronic ground state and of the corresponding pure solvent is shown in the inset. Both spectra are normalized to the intensity of the solvent lines at 385 cm^{-1} and at at 802 cm^{-1}.

Obviously in the range 1050 to 2000 cm^{-1} the excited state CARS spectrum exhibits a completely changed pattern compared to the electronic ground state, indicating a changed geometry. As a specific feature of CARS under electronic resonance conditions, vibrational resonances occur as asymmetric dips (i.e., $C < 0$, $B > 0$) on a strong four-wave mixing background as has been discussed in section 4. It is interesting to note that compared to the frequencies of the C═C stretching region around 1600 cm^{-1} in the electronic ground state there are strong vibrational resonances which are either downshifted (probably as a result of a decreased C═C bond order in the excited state) or unusually upshifted (as a result of dominating S_0-S_1 vibronic coupling) in their vibrational frequencies. Two unusually upshifted asymmetric minima near 1620 and 1780 cm^{-1} (marked by thick arrows), which are strongly frequency broadened, can be clearly distinguished. In addition, these two vibrational bands show an unusually strong frequency dependence on the solvent being observed for these bands exclusively.[24] The vibrational frequencies of the two bands have been determined for DPH dissolved in neat solvents and in mixtures of solvents differing in their polarizabilities, polarities, and viscosities as well. We did not find any systematic dependence on solvent polarity or on viscosity (cf. Figure 3A,B). A plot of the frequencies versus the polarizability is presented in Figure 4. The polarizability of the solvent is calculated from the refractive index n of the liquid from $(n^2 - 1)/(n^2 + 2)$. It can been seen that both vibrations are shifted to lower frequencies as the polarizability of the solvent is increased.

Figure 5 shows the kinetics of the rise of the excited state vibrational resonances in the region 1470 to 2000 cm^{-1} immediately after UV excitation using pulses of 2 ps duration and different delays between excitation and CARS probing. Within the accuracy of the measurement all dips in the spectrum

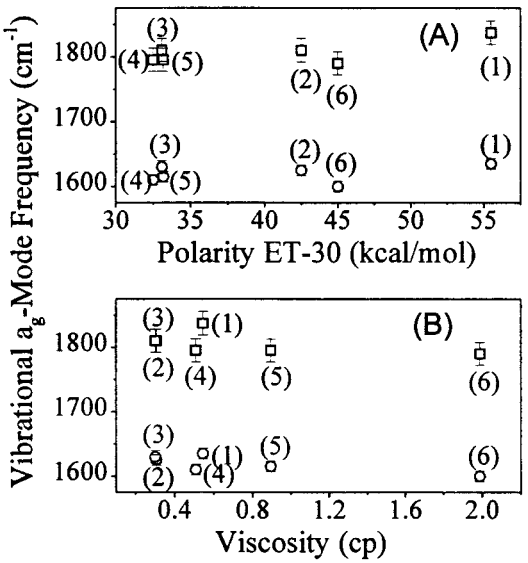

Figure 3. (A) Dependences of the two vibrational frequencies (□, ○) above 1600 cm^{-1} of the excited electronic state of DPH on the polarity of the solvents (1) methanol, (2) acetone, (3) hexane, (4) octane, (5) cyclohexane, (6) dimethyl sulfoxide. (B) Dependences of the two vibrational frequencies (□, ○) above 1600 cm^{-1} of the excited electronic state of DPH on the viscosity of the solvents (1) methanol, (2) acetone, (3) hexane, (4) octane, (5) cyclohexane, (6) dimethyl sulfoxide.

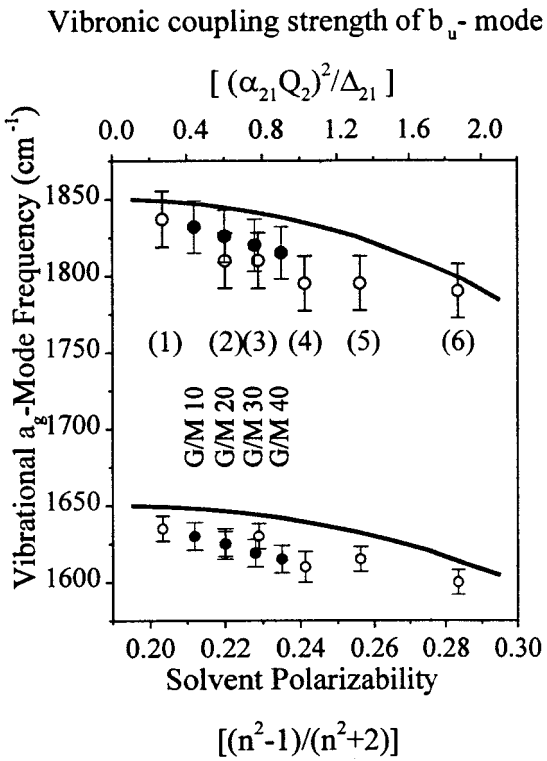

Figure 4. Dependences of the vibrational frequencies above 1600 cm^{-1} of the excited electronic state of DPH on the polarizabillity of neat solvents (○) and of mixtures of glycerol and methanol (●). [(1) methanol, (2) acetone, (3) hexane, (4) octane, (5) cyclohexane, (6) dimethyl sulfoxide; G/M 10 = 10 vol % glycerol in methanol, G/M 20 = 20 vol % glycerol in methanol, etc.] Straight lines represent calculated frequency dependences on the vibronic coupling strength of the b_u mode between the excited electronic states.

grow simultaneously with a rise time limited by our instrumental response. Their relative magnitude remains unchanged up to the longest delays of 200 ps.

In Figure 6A, a CARS spectrum in the frequency range 1000 to 1200 cm^{-1} of DPH dissolved in cyclohexane photoexcited by the UV pulse (solid line) is shown together with a spectrum of the same sample which is not irradiated by the UV pulse (dotted line). In the latter case, cyclohexane CARS lines can be observed only. CARS lines of DPH are not visible due to

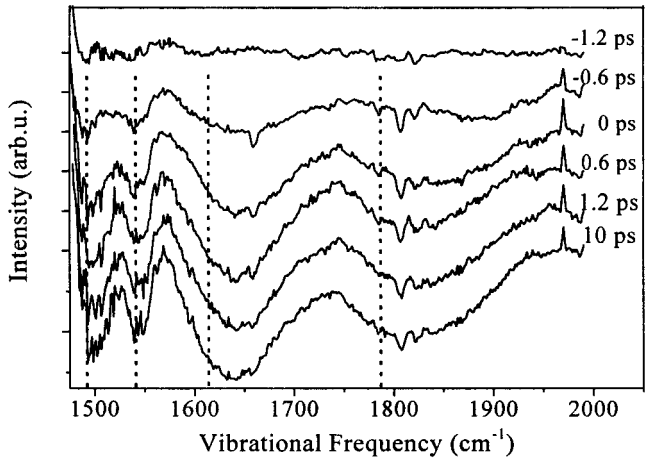

Figure 5. CARS spectra of the excited singlet state of DPH (10^{-3} mol/L dissolved in cyclohexane, $\lambda_{UV} = 370$ nm, $\lambda_1 = 740$ nm) recorded with different delays after photoexcitation. Dashed lines represent guide lines for the vibrational resonances at 1490, 1542, 1620, and 1720 cm^{-1} respectively.

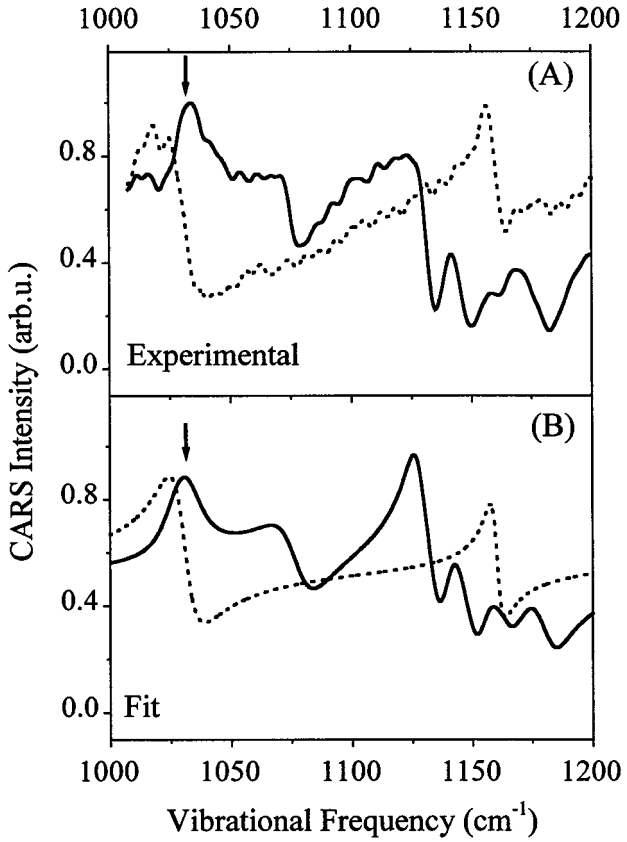

Figure 6. (A) Change of the shape of the cyclohexane CARS line at 1030 cm^{-1} (indicated by an arrow) due to the electronic hyperpolarizability of the first excited state of DPH (5×10^{-4} mol/L dissolved in cyclohexane, $\lambda_1 = 720$ nm). Solid line: CARS spectrum of DPH with UV excitation $\lambda_{UV} = 355$ nm. Dotted line: without UV excitation. (B) Fits of the CARS line shapes of DPH in the first excited singlet state (solid line) and of pure cyclohexane (dotted line). Parameters used for the fit are given in Table 2. A relative concentration of DPH molecules in the excited state of $N_{\text{excited state}}/N_{\text{cyclohexane}} \cong 2 \times 10^{-5}$ is estimated from a bleaching measurement of the sample at 355 nm.

TABLE 1: Bond Lengths between Neighboring C Bonds[a] of the Chain (given in Å) for the Three Lowest Singlet States of DPH Calculated by MOPAC-93[41]

electronic state	bond length (Å)						
	C_1-C_2	C_2-C_3	C_3-C_4	C_4-C_5	C_5-C_6	C_6-C_7	C_7-C_8
1^1A_g	1.46	1.34	1.45	1.34	1.45	1.34	1.46
1^1B_u	1.43	1.37	1.41	1.38	1.41	1.37	1.43
2^1A_g	1.41	1.41	1.37	1.44	1.37	1.41	1.41

[a] Numbering of C atoms is given in Figure 1.

TABLE 2: Fit Parameters Used for Approximation of the CARS Spectra in Figure 4a and 4b[a]

	ω (cm^{-1})	Γ_R (cm^{-1})	R/Γ_R	J/Γ_R
Cyclohexane	1030	5	0.5	0
	1160	3	0.4	0
	1270	5	0.7	0
$DPH_{excited\ state}$[b]	1077	8	−10 000	20 000
	1131	4	−27 000	55 000
	1145	4	−23 000	46 000
	1160	5	−13 000	26 000
	1180	5	−13 000	26 000
	1240	17	−18 000	17 000

[a] Parameters are normalized to the electronic hyperpolarizability of cyclohexane $\gamma_{cyclohexane} \equiv 1$ and based on a relative concentration of DPH in the first excited singlet state $N_{excited\ state}/N_{cyclohexane} \cong 2 \times 10^{-5}$. [b] Real and imaginary part of the electronic contribution to γ^{FWM}_{solute} are $b' = -50\,000$ and $b'' = 75\,000$, respectively.

their too low concentration (5×10^{-4} mol/L). After irradiation, CARS lines from the excited state can be detected due to resonance enhancement by the transient absorption. Additionally, the amplitudes of cyclohexane CARS lines decrease relative to the enhanced four wave mixing background, and their shape changes as well. This is a clear indication for an enhanced third-order hyperpolarizability γ_{S1} originating from the excited electronic state of DPH. It can be studied in the case of the cyclohexane Raman resonance at 1030 cm^{-1} (indicated by an arrow), which does not interfere with neighboring resonances originating from the excited state of DPH. For determination of γ_{S1} we carried out a CARS line shape analysis around this CARS line. The fit was carried out in three steps:

(i) $((\gamma_R/\Gamma_R)/\gamma)_{cyclohexane}$ of the different cyclohexane Raman lines was obtained from the pure solvent spectrum with γ and γ^R being positive and real quantities. The fit of the spectrum of pure cyclohexane (dotted line) is shown in Figure 5B (dotted line).

(ii) The complex excited electronic state hyperpolarizability of DPH $\gamma_{excited\ state} \equiv (b' - ib'')_{excited\ state}$ was determined by a fit of the isolated solvent CARS line at 1030 cm^{-1}, which changes its shape and its relative strength with respect to the background after UV excitation due to interference between the $\gamma_{excited\ state}$ and $\gamma^{FWM}_{cyclohexane}$ contributions.

(iii) Taking into account the complex valued electronic contribution of DPH, as determined in the previous step, the CARS line shapes of excited state DPH were fitted by complex Raman contributions $\gamma_R \equiv R_R - iJ_R$ to get their frequencies and intensities. For the fit, equal ratios J_R/R_R for the vibrations of the excited state have been assumed within the spectrum. This assumption is reasonable if electronic resonance conditions are only slightly changing within the tuning range.[34] The fitted CARS spectrum is shown in Figure 6B (solid line); the corresponding fitting parameters are summarized in Table 2.

For determination of the absolute value of γ_{S1} we determined the concentration of molecules in the first excited singlet state from the bleaching of the absorption band at 355 nm upon UV irradiation. The transient absorption of DPH at 355 nm from the lowest excited states to higher levels can be ignored.[9] A relative concentration of $N_{excited\ state}/N_{cyclohexane} \cong 2 \times 10^{-5}$ is estimated assuming that bleaching of the electronic ground state results in population of the long-lived first excited singlet state exclusively. Spatial distributions of the excited states within the irradiated volume have not been considered for simplicity. From the known absolute value of the third order hyperpolarizability of cyclohexane $\gamma_{cyclohexane} = 3.02 \times 10^{-36}$ esu[37] we derive an excited state hyperpolarizability of $|\gamma_{S_1}| \cong 2.7 \times 10^{-31}$ esu.

6. Discussion

6.1. Excited State Hyperpolarizability. The huge excited state hyperpolarizability $|\gamma_{S_1}| \cong 2.7 \times 10^{-31}$ esu is measured under electronic resonance conditions with the transient absorption band. Resonance conditions are also clearly indicated by the strong imaginary contribution to the excited state hyperpolarizability b'' (cf. Table 2). The increase of optical nonlinearity by 1 order of magnitude[40] compared to that of trans-stilbene determined under similar (electronic resonance) conditions can be explained by the increased length of the excited chain. The high value measured under electronic resonance conditions also indicates an enhanced off-resonant hyperpolarizability of the excited electronic state of DPH compared to that in the electronic ground state. The enhancement of the hyperpolarizability near a one-photon resonance can be roughly described by $1/(\Delta\omega + \Gamma_{EL})^2$, where $\Delta\omega$ is the detuning of CARS frequencies from the absorption frequency of a spectral width of Γ_{EL}.[32] Taking into account a spectral width of the transient absorption near 650 nm of about 1500 cm^{-1},[27] a hyperpolarizability $\gamma_{STAT} \cong 10^{-33}$ esu can be estimated in the static limit (i.e., at zero frequency).[32] The latter considerably exceeds the off-resonant value $\gamma \leq 5 \times 10^{-35}$ esu of the molecule in the electronic ground state measured at 1064 nm excitation.[9]

It is interesting to note that the value of the excited state hyperpolarizability of DPH is comparable or even higher than those of polymethines of comparable size measured in the electronic ground state.[32] According to our calculations (see section 6.2) the bond length alternation is significantly reduced in both excited singlets becoming a more polymethine-like structure. Therefore, we suggest to attribute the enhanced hyperpolarizability to the increased delocalization of the π-electrons in the chain.

6.2. Model of S_1-S_2 Vibronic Coupling by an Asymmetric Low Frequency Mode. The other important findings are the two vibrational frequencies that are upshifted above 1600 cm^{-1} in contrast to the behavior which is normally expected if the bond order in the C=C stretching region is decreased after excitation. Only the totally symmetric stretching motion of the chain is known to exhibit such a strong upshift due to $1A_g-2A_g$ (S_0-S_1) vibronic coupling, and we assign both upshifted bands to the same totally symmetric vibrational motion. Increasing polarizability of the solvent narrows the gap between the excited electronic states and consequently their solvent dependent frequency shifts give evidence of an additional S_1-S_2 vibronic coupling effect. If the molecule keeps planar configuration and the C_{2h} symmetry is maintained in the excited state, coupling between the $2A_g$ and $1B_u$ states by the a_g mode is symmetrically forbidden. Thus, two mechanisms are possible to cause vibronic coupling between the $2A_g$ and the $1B_u$ states: (i) distortion of symmetry and (ii) pertubation due to a b_u-type vibrational mode.

(i) Two vibrational frequencies of the same vibrational mode could originate from two different species (e.g., two rotamers) in the $2A_g$ state, both deviating from C_{2h} symmetry (e.g., due to twisting of the backbone). In this case, vibronic coupling by an a_g mode is not strictly forbidden[18] and conformational

dependent coupling constants can generate two frequencies belonging to the same C=C stretching motion for the two species. Because of the very small gap, even with rather small coupling constants, vibronic coupling can be quite effective. Both vibrations are expected to shift down with decreasing gap between the two excited electronic states. Frequency broadening can be caused by conformational distributions around the two equilibrium geometries. Other vibrational modes which do not couple the two excited electronic states are expected neither to be shifted in solvents of different polarizabilities nor unusually frequency broadened due to conformational distributions.

However, according to our electronic structure calculations (MOPAC93[41]) and the pronounced π-electron delocalization, diphenylhexatriene is planar in the electronic ground and as well in both excited electronic states, maintaining C_{2h} symmetry. Even if there are deviations from strict C_{2h} symmetry (e.g., due to interaction with the solvent), two upshifted vibrations are indicative for two separate species. This variant is rather unlikely because the observed kinetics (rise of the CARS lines originating from S_1[24] and fluorescence decay[30]) give no hints for two separate species in the excited state.

(ii) For strict C_{2h} symmetry, frequency changes of the totally symmetric C=C mode can be caused by coupling via a b_u-type vibrational mode of the chain. Taking into account the small energetic gap, this effect can become significant, especially as a C−C bond length reversal occurs between the excited states.

The calculated bond lengths r_i between neighboring C_i atoms of the chain are given in Table 1. As typical for polyenes,[42] the ground state exhibits a distinct degree of bond length alternation ($BLA = 2r_{i+1} - r_i/r_{i+1} + r_i \cong 0.08$) between neighboring bonds in the chain. For the $1B_u$ state we calculated a decreased BLA $\cong$ 0.02. In the $2A_g$ state, bond alternation also decreases with respect to the ground state but there is a bond length reversal. As these geometrical changes of the chain correspond to the motion of the totally symmetric C=C stretching vibration with antiphase elongations of neighboring C=C bonds there are strong origin shifts for the totally symmetric C=C stretching vibration between both excited electronic states $2A_g$ and $1B_u$. In addition, rather strong origin shifts are calculated for the lowest b_u mode for the $2A_g$ and $1B_u$ state, respectively. Its calculated frequency of 40 cm^{-1} in the electronic ground state fairly well corresponds to those of the strong low frequency mode of the Raman spectrum at 35 cm^{-1} (see inset of Figure 2).[25] This mode is known to be effective in vibronic coupling between the excited electronic states in a polyene.[17] Due to its asymmetric motion, it is able to influence the potential of the totally symmetric C=C stretching mode of the chain and hence the corresponding frequency as well. This mechanism is quantified in a model taking into account the two excited electronic singlet states and the two modes belonging to the a_g and b_u symmetry species, respectively.[25]

Within the harmonic approximation the diabatic potentials for the two (uncoupled) excited singlet states can be written:

$$V_{2Ag}(Q_1,Q_2) = \frac{1}{2}[\omega^2_{1\_2Ag}(Q_1 - Q_{1\_2Ag})^2 + \omega_2^2 Q_2^2] \quad (4)$$

$$V_{1Bu}(Q_1,Q_2) = \frac{1}{2}[\omega^2_{1\_1Bu}(Q_1 - Q_{1\_1Bu})^2 + \omega_2^2 Q_2^2] + \Delta_{12} \quad (5)$$

where Q_1 and Q_2 are the elongations of the a_g mode and of the b_u mode, respectively, Q_{1_2Ag} and Q_{1_1Bu} are the positions of the diabatic minima of the corresponding potentials (mass normalized origin shifts), and Δ_{12} is the gap between the two minima. Vibronic coupling between the states is performed by

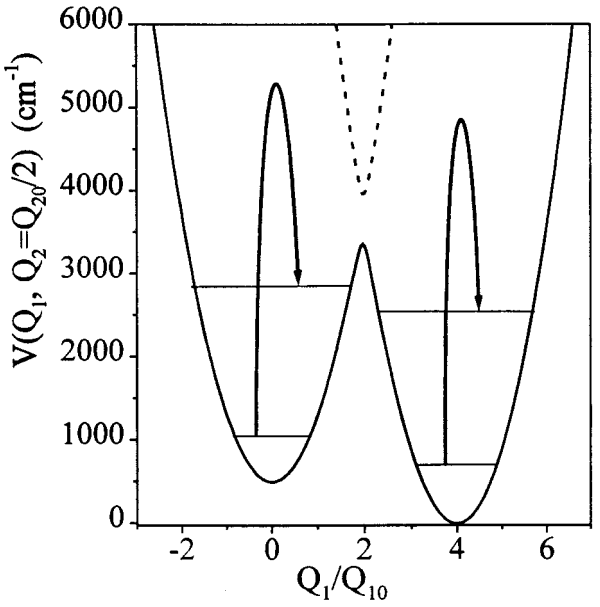

Figure 7. Effective potential for the totally symmetric C=C − stretching coordinate around 1700 cm^{-1} in the lowest excited singlet state. The position of the second state resulting from vibronic coupling is shown as dashed line. In the $2A_g$ state the pseudo-Jahn−Teller effect leads to a double-well potential. An effective amplitude of the coupling mode $Q_2 = Q_{20}/2$ is assumed (Q_{20}: zero-point oscillation of the Q_2 mode, abscissa values of Q_1 elongation normalized to the zero-point oscillation Q_{10}). Horizontal lines indicate the energy positions for the lowest vibrational levels in the respective diabatic potentials (left $1B_u$ section, right $2A_g$ section). The assumed Raman transitions are indicated.

a linear coupling ansatz $V_{2Ag,1Bu} = \alpha_{12}Q_2$. The coupling constant α_{12} is estimated from the PPP method to be 1 order of magnitude lower than the α_{01} constant. For the latter we take the value derived in ref 11: $|\alpha_{01}| = 1.65$ eV $Å^{-1}amu^{-1/2}$.

Coupling results in the two-dimensional potential:

$$V(Q_1,Q_2) = \frac{V_{2Ag} + V_{1Bu}}{2} - \sqrt{\left(\frac{V_{2Ag} - V_{1Bu}}{2}\right)^2 + (\alpha_{12}Q_2)^2} \quad (6)$$

Under these conditions a double-well potential along the Q_1 coordinate in the first excited singlet state is generated by a pseudo-Jahn−Teller mechanism. It arises from coupling of both potentials (eq 4 and eq 5) in assuming a sufficiently large shift between the minima $d = (Q_{1\_2Ag} - Q_{1\_2Bu})/\sqrt{m_1^{\text{eff}}}$. For an estimated value of $d = 0.18$ Å, two minima arise in the potential of the lowest excited singlet state which result in two quasi-bound vibrational levels around the Q_{1_2Ag} and Q_{1_2Bu} minima positions (cf. Figure 7).

The observed dependence of vibrational frequencies on the solvent polarizability can be explained by the following considerations. In transparent solvents, the effective vibronic coupling between the excited states in the first approximation varies with the Lorenz−Lorentz molar refraction according to the relation

$$\frac{\alpha_{12}^2}{\Delta_{12}} = \left[\frac{\alpha_{12}^2}{\Delta_{12}}\right]_{\text{vacuum}} \left(1 + \beta\frac{n^2 - 1}{n^2 + 2}\right) \quad (7)$$

The equation is derived applying Hudson's rule[22] for the dependence of the effective coupling element α_{12}/Δ_{12} on solvent refractive indices n. Here, β is a positively valued parameter

related to the transition dipole and polarizability properties of the solute molecule. Applying eq 7 in combination with eq 6, the observed frequency shifts versus solvent polarizabilty (cf. Figure 4) are reproduced qualitatively.

The two minima arise from the originally diabatic potentials of the $2A_g$ and of the $1B_u$ potentials. This also explains the close correspondence of the two vibrational frequencies measured in DPH either to the excited state frequency observed in diphenyloctatetraene at 1755 cm^{-1} (assigned to the $2A_g$ state[19]) or to the band in DPB at 1620 cm^{-1} measured after electronic excitation which has been assigned to the $1B_u$ or to a mixed $1B_u/2A_g$ state.[20]

Taking into account that the curvature of the potential of the Q_1 mode is modulated by anharmonic coupling with the Q_2 mode, a strong frequency broadening is expected. Within the simplest model the oscillations are interrupted with the cycle of the low frequency mode, resulting in a broadening of $\Delta\omega_1 = \omega_2$. The other modes, which are not coupled, can be described by independent normal coordinates and should neither be shifted by changing the polarizability of the solvent nor should they be unusually broadened. Modulation of the saddle point between the two minima by the Q_2 vibration is able to transfer the wave packet of the Q_1 mode from one minimum to the other, promoting a fast relaxation.

7. Conclusions

In conclusion, we have derived an extremely high third order hyperpolarizability $\gamma_{\text{excited state}} \cong 3 \times 10^{-31}$ esu from the time-resolved CARS spectra of the first excited singlet state of DPH. According to estimations, the nonlinearity of the first excited singlet state of DPH under off-resonant excitation is strongly enhanced compared to the electronic ground state as well. Supported by the close correspondence to the hyperpolarizabilities of polymethines and by the calculated decrease in bond length alternation of the chain, we suggest that the increased delocalization of π-electrons in the chain after excitation, i.e., the more polymethine-like structure is a main reason for enhancement of the optical nonlinearity in the excited state of this polyene.

Furthermore, we observed a strong S_1-S_2 vibronic coupling effect in the first excited state of the molecule. It may be explained assuming coexistence of two species in the $2A_g$ state.

More likely, coupling is attributed to the action of low frequency asymmetric vibrational motions of the molecule influencing the potential of the totally symmetric C═C stretching normal coordinate of the chain. According to this model, coupling by a low frequency asymmetric mode generates a double minimum for the C═C stretching coordinate in the lowest excited singlet state, and consequentely two frequencies originate from this mode. Coupling to the low frequency mode leads to strong frequency broadening of the C═C stretching bands.

Extension of the experiments from the frequency to the time domain where, on a femtosecond time scale, coupling phenomena can be investigated in a more direct way[43] and should lead to a refined understanding of the vibronic coupling mechanisms involved in fast radiationless energy transfer.

Acknowledgment. We are very grateful to Ms. B. Neutenkoetter for technical support. We also thank Dr. P. Hamm for valuable discussions. Support of the Deutsche Forschungsgemeinschaft (project No.: We 1489/5-1) is gratefully acknowledged.

References and Notes

(1) Wald, G. *Science* **1962**, *162*, 230.
(2) Young, A. J.; Frank, H. A.; *J. Photochem. Photobiol. B: Biology* **1996**, *36*, 3.
(3) Maxpherson, A. N.; Gillbro, T. *J. Phys. Chem. A* **1998**, *102*, 5049.
(4) Connelly, J. P.; Müller, M. G.; Bassi, R.; Croce, R.; Holzwarth, A. R.; *Biochemistry* **1997**, *36*, 281.
(5) Flytzanis, C. In *Nonlinear optical properties of organic molecules and crystals*; Chemla, D. S., Zyss, J., Eds.; Academic Press: New York, 1987; Vol. 2.
(6) Bredas, J. L.; Adam, C.; Taaks, P.; Persoons, A. *Chem. Rev.* **1994**, *94*, 243.
(7) Marder, S. R.; Perry, J. W.; Bourhill, G.; Tiemann, B. G.; Masour, K. *Science* **1993**, *261*, 186.
(8) Rodenberger, D. C.; Heflin, J. R.; Garito, A. F. *Nature* **1992**, *359*, 309.
(9) Rodenberger, D. C.; Heflin, J. R.; Garito, A. F. *Phys. Rev. A* **1995**, 51−4, 3234.
(10) Auerbach, R. A.; Christensen, R. L.; Granville, M. F.; Kohler, B. E. *J. Chem. Phys.* **1981**, *74*, 4.
(11) Orlandi, G.; Zerbetto, F.; Zgierski, M. Z. *Chem. Rev.* **1991**, *91*, 867.
(12) Hudson, B. S.; Kohler, B. E. *J. Chem. Phys.* **1973**, *59*, 4984.
(13) Hudson, B. S.; Kohler, B. E.; Schulten, K. In *Excited States*; Lim, E. C., Ed.; Academic Press: New York, 1982; Vol. 6, p 1.
(14) Ithoh, T.; Kohler, B. E. *J. Phys. Chem.* **1987**, *91*, 1760.
(15) Nagae, H.; Kuki, M.; Zhang, J.-P.; Sashima, T.; Mukai, Y.; Koyama, Y.; Proceedings of the 9th International Conference on Time-Resolved Vibrational Spectroscopy, May 16−21, 1999.
(16) Shreve, A. P.; Trautmann, T. K.; Frank, H. A.; Owens, T. G.; Albrecht, A. C. *Biochim. Biophys. Acta* **1991**, *1058*, 280.
(17) Pfanstiel, J. F.; Champagne, B. B.; Majewski, W. A.; Plusquellic, D. F.; Pratt, D. W. *Science* **1989**, *245*, 737.
(18) Noguchi, T.; Hayashi, H.; Tasumi, M.; Atkinson, G. H. J. *J. Phys. Chem.* **1991**, *95*, 3167.
(19) Kasama, A.; Taya, M.; Kamisuki, T.; Adachi, Y.; Maeda, S. In *Time-Resolved Vibrational Spectroscopy*; Atkinson, J., Ed.; Gordon and Breach: New York, 1987; p 304.
(20) Morris, D. L.; Gustafson, T. L. *Appl. Phys. B* **1994**, *59* 389.
(21) Bachilo, S. M.; Spangler, C. W.; Gillbro, T. *Chem. Phys. Lett.* **1998**, *283*, 235.
(22) Andrews, J. R.; Hudson, B. S. *J. Chem. Phys.* **1978**, *68*, 4587.
(23) Hogiu, S.; Werncke, W.; Pfeiffer, M.; Lau, A.; Steinke, T. *Chem. Phys. Lett.* **1998**, *287*, 8.
(24) Hogiu, S.; Werncke, W.; Pfeiffer, M.; Lau, A. *Chem. Phys. Lett.* **1999**, *303*, 218.
(25) Pfeiffer, M.; Werncke, W.; Hogiu, S.; Kummrow, A.; Lau, A. *Chem. Phys. Lett.* **1998**, *295*, 56.
(26) Atom Yee, W.; O'Neil, R. H.; Lewis, J. W.; Zhang, J. Z.; Kliger, D. S.; *Chem. Phys. Lett.* **1997**, *276*, 430.
(27) Goldbeck, R. A.; Tarowski, A. J.; Russel, E. L.; Rice, J. K.; Birge, R. R.; Switkes, E.; Kliger, D. S. *J. Chem. Phys.* **1982**, *77*, 3319.
(28) Saltiel, J.; Ko, D. H.; Fleming, A. *J. Am. Chem. Soc.* **1994**, *116*, 4099.
(29) Fang, H. L. B.; Trash, R. L.; Laroi, G. E. *Chem. Phys. Lett.* **1978**, *57*, 59.
(30) Parasassi, T.; De Stasio, G.; Rusch, R. M.; Gratton, E. *Biophys. J.* **1991**, *59*, 466.
(31) Oudar, J. L.; Smith, R. W.; Shen, Y. R. *Appl. Phys. Lett.* **1979**, *34*, 758.
(32) Werncke, W.; Pfeiffer, M.; Lau, A.; Grahn, W.; Johannes, H.-H.; Dähne, L. *J. Opt. Soc. Am. B* **1998**, *15*, 863.
(33) Nibler, J. W.; Knighten, G. V. In *Raman Spectroscopy of Gases and Liquids, Topics in Current Physics 1*; Weber, A., Ed.; Springer: Berlin, 1979; pp 253−299.
(34) Pfeiffer, M.; Lau, A.; Werncke, W. *J. Raman Spectrosc.* **1984**, *15*, 20.
(35) Fleming, J. W.; Johnson, C. S. *J. Raman Spectrosc.* **1979**, *8*, 284.
(36) Pfeiffer, M.; Lau, A.; Werncke, W. *J. Raman Spectrosc.* **1986**, *17*, 425.
(37) Kajzar, F.; Messier, J. *Phys. Rev. A* **1985**, *32*, 2352.
(38) Achmanov, S. A.; Bunkin, A. F.; Ivanov, S. G.; Koroteev, N. I. *Sov. Phys. JETP* **1978**, *47*, 667.
(39) Brakel, R.; Schneider, F. W. In *Advances in Non-linear Spectroscopy*; Clark, R. J. H., Hester, R. E., Eds.; John Wiley: Chichester, 1988; Vol. 15, p 149.
(40) Koroteev, N. I.; Shkurinow, A. P.; Toleutaev, B N. In *Coherent Raman Spectroscopy*; Marowski, G., Smirnow, V. V., Eds.; Springer Proceedings in Physics 63; Springer-Verlag: Berlin, 1992; p 186.
(41) MOPAC 93, Fujitsu Limited, Tokyo, Japan, 1993.
(42) Klessinger, M. *J. Mol. Struct.* **1992**, *266* 53.
(43) Kobayashi, T.; Shirakawa, A. Proceedings of the 9th International Conference on Time-Resolved Vibrational Spectroscopy, May 16−21, 1999.